Low Cloud Type over the Ocean from Surface Observations. Part II: Geographical and Seasonal Variations

JOEL R. NORRIS*

Department of Atmospheric Sciences, University of Washington, Seattle, Washington

(Manuscript received 10 October 1996, in final form 4 June 1997)

ABSTRACT

Synoptic surface cloud observations primarily made by volunteer observing ships are used to construct global climatologies of the frequency of occurrence of individual low cloud types over the ocean for daytime during summer and winter seasons for the time period 1954–92. This essentially separates the previous S. Warren et al. ''stratus,'' ''cumulus,'' and ''cumulonimbus'' climatologies into their constituent cloud types. The different geographical and seasonal distributions of low cloud types indicate that each type within the Warren et al. categories is associated with different meteorological conditions. Hence, investigations based on individual low cloud types instead of broader categories will best identify the processes and variability in meteorological parameters responsible for observed variability in cloudiness. The present study is intended to provide a foundation for future investigations by documenting the climatological distributions of low cloud type frequency and demonstrating the physical consistency with expected patterns of boundary layer structure, advection, surface divergence, and synoptic activity over the global ocean.

Further analyses are conducted to examine in greater detail transitions in low cloud type and related boundary layer processes in the eastern subtropical North Pacific, eastern equatorial Pacific, and western North Pacific during summer. Maxima in the climatological frequencies of stratocumulus, cumulus-with-stratocumulus, and cumulus occur progressively equatorward over eastern subtropical oceans, consistent with an increasing decoupled boundary layer. This transition is also observed north of the equatorial cold tongue, but advection over colder SST on the southern side of equatorial cold tongue sometimes produces an absence of low cloudiness. A transition between cumuliform low cloud types to the south and stratiform low cloud types to the north occurs over the region of strong SST gradient in the western North Pacific, and during summer the maximum frequency of stratus associated with precipitation is collocated with the region of strong SST gradient.

1. Introduction

One of the greatest challenges in understanding climate variability and climate change is determining the role of cloudiness, both in terms of its influence on the radiation budget and its dependence on other parameters of the climate system (Arking 1991). Several datasets based on satellite or synoptic surface observations have been developed to study variability in cloudiness over the global ocean, such as the International Satellite Cloud Climatology Project (ISCCP) (Rossow and Schiffer 1991), the Comprehensive Ocean–Atmosphere Data Set (COADS) $2° \times 2°$ monthly summaries (Woodruff et al. 1987), and the Warren et al. (1988) (hereafter W88) dataset. Satellite-based datasets have the advantages of high resolution, global coverage, and quantitative radiative information, but are available only for a short period of record (since 1983 for ISCCP). Hence, it is necessary to use surface-based datasets to investigate variability in cloudiness at interannual and longer timescales with statistical reliability.

Hanson (1991) and Klein et al. (1995) used COADS total cloud cover to examine interannual variability in cloudiness, sea surface temperature (SST), and lower-tropospheric static stability in eastern subtropical stratocumulus regions, and Deser and Wallace (1990) used COADS total cloud cover to examine El Niño–Southern Oscillation (ENSO) variability of cloudiness over the eastern equatorial Pacific. Norris and Leovy (1994) used W88 ''stratus'' cloud amount to examine interannual variability in marine stratiform cloudiness and SST over the global ocean. However, studies such as these, which use total cloud cover or other broad categories of cloudiness, are handicapped by the fact that various types of cloudiness within the category form by different processes and therefore may respond differently to the same forcing. For example, low stratiform cloudiness decreases but deep convective cloudiness increases over the eastern equatorial Pacific during the warm phase of ENSO; these two responses compensate for each other in the total cloud cover signal. Even more limited categories such as stratus from W88 suffer from this prob-

*Current affiliation: National Center for Atmospheric Research, Boulder, Colorado.

Corresponding author address: Joel R. Norris, NCAR/ASP, P.O. Box 3000, Boulder, CO 80307-3000.
E-mail: jnorris@ucar.edu

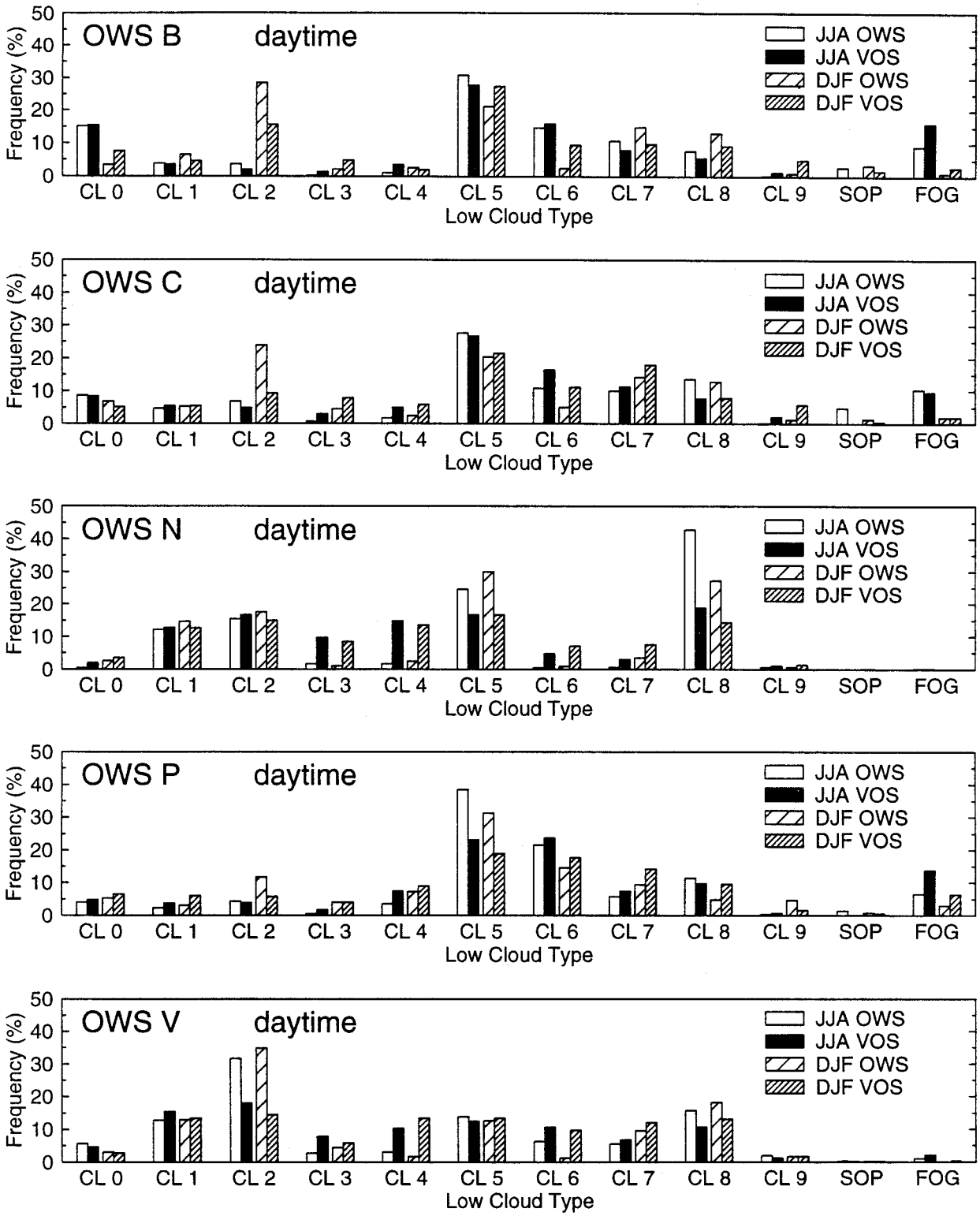

FIG. 1. Daytime frequency of occurrence of the low cloud types described in Table 1 of Part I along with sky-obscuring precipitation (SOP) and sky-obscuring fog (FOG) for OWS B (56.5°N, 51°W), C (52.75°N, 35.5°W), N (30°N, 140°W), P (50°N, 145°W), and V (34°N, 164°E) and nearby VOS during JJA and DJF. VOS observations are from a 2° × 2° box centered on the OWS. Both OWS and VOS data are from the time period 1954–72. Color coding of bars: white—OWS JJA; black—VOS JJA; light hatching—OWS DJF; dense hatching—VOS DJF.

TABLE 1. Correspondence between W88 low cloud categories and low cloud types in the present study.

W88 categories	Low cloud types in the present study
Stratus	C_L 4, C_L 5, C_L 6, C_L 7, C_L 8, sky-obscuring fog
Cumulus	C_L 1, C_L 2
Cumulonimbus	C_L 3, C_L 9

TABLE 2. Global mean and geographical standard deviation of low cloud type amount-when-present during daytime.

C_L	AWP (%)
1	33.8 ± 8.7
2	45.2 ± 10.0
3	53.4 ± 11.2
4	57.8 ± 11.2
5	75.0 ± 9.8
6	81.0 ± 11.5
7	80.4 ± 9.2
8	68.8 ± 10.5
9	62.6 ± 13.3

lem. The W88 stratus category includes fair-weather stratus, bad-weather stratus, stratocumulus, cumulus with stratocumulus, and sky-obscuring fog, each of which is associated with different meteorological conditions at midlatitudes (Norris 1998).

This paper proposes that the use of a dataset divided into individual cloud types can best identify the processes and variability in meteorological parameters responsible for observed variability in cloudiness. Synoptic surface observations are most useful for this purpose since human observers identify clouds by morphological type and therefore qualitatively describe the processes influencing cloud type. Satellite-based datasets are less useful for this purpose since they use radiative characteristics (e.g., cloud-top temperature and cloud optical thickness) to identify cloud type, which often poorly corresponds to the surmised morphological type, particularly for low cloud types (S. Warren 1996, personal communication). Analysis of data from the Earth Radiation Budget Experiment and ISCCP shows that low cloudiness makes the largest contribution to global net cloud radiative forcing (Hartmann et al. 1992); therefore, low cloud types will be the focus of the present study. Since global distributions of individual low cloud types from synoptic surface observations have been previously calculated only for two seasons of a single year (Hahn et al. 1988), Part II of this study will present climatological distributions of nine low cloud types and three additional categories during summer and winter as a baseline for future interannual studies. Aside from differences in diurnal sampling and the averaging time period, these climatologies essentially separate the W88 stratus, cumulus, and cumulonimbus climatologies into their constituent cloud types. Illustrations of transitions in low cloud type and related climate parameters will also be provided for the eastern subtropical North Pacific, eastern equatorial Pacific, and western North Pacific. The results from Part I (Norris 1998), which documented typical marine boundary layer (MBL) structures and surface meteorological conditions associated with various low cloud types at several ocean weather stations (OWS) located in the midlatitude and eastern subtropical oceans, will be used to help interpret the results of the present study.

2. Data

The source of data used in this study is an updated version of the Edited Cloud Report Archive (Hahn et al. 1996), a collection of individual synoptic surface cloud and meteorological observations obtained from the COADS Compressed Marine Reports and Long Marine Reports archives. Volunteer Observing Ships (VOS) contributed the large majority of the 60 million observations available over most of the global ocean during the time period 1954–92. These are the same observations from which the W88 dataset was constructed for the time period 1952–81. Observations before 1954 were not used in the present study because they inconsistently identify cloud type (W88). As described previously in Part I (Norris 1998), surface observers classify low cloudiness into 10 different types (including no-low-cloud) according to the synoptic code (WMO 1975). Table 1 from Part I gives nontechnical descriptions of each low cloud type and its priority in designating the low type code (C_L) if more then one cloud type is present. Since the low cloud type code allows only one cloud type to be reported, the occurrence of lesser-priority cloud types may be underestimated. For the purposes of this paper, sky-obscuring fog and sky-obscuring precipitation, diagnosed by the present-weather code (WMO 1974), are identified as two additional ''low cloud types.'' These 12 types include every possible sky condition for low cloud identification. Overlooking a few unimportant definitional differences with W88, Table 1 shows the correspondence between the W88 low cloud categories and the low cloud types presented in this paper.

VOS observers did not receive as much training as the OWS observers who provided the data used in Part I, and they sometimes identify cloud type differently. Figure 1 compares the daytime frequency of occurrence of each cloud type calculated from OWS observations to that from nearby VOS observations during June–August (JJA) and December–February (DJF). Only VOS observations made within a $2° \times 2°$ box centered on the OWS were used, and both OWS and VOS observations are from the time period 1954–72. Although OWS and VOS observers generally agree on which cloud types are most frequent and which are least frequent, the VOS observers tend to identify the more frequently occurring cloud types less often and the less frequently occurring cloud types more often than do OWS observers. This tendency is consistent with increased random errors in

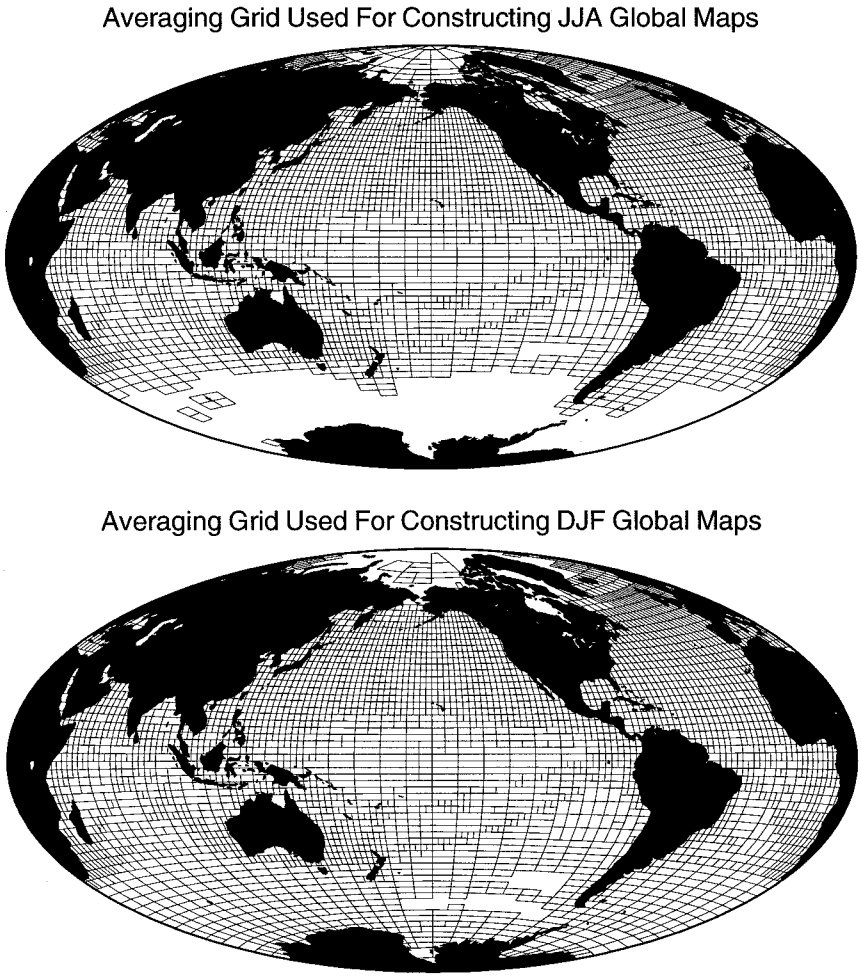

FIG. 2. Averaging grid used for constructing global climatologies of low cloud type JJA (top) and DJF (bottom) daytime FQ. Grid boxes with less than 100 observations contributing are omitted.

cloud identification by less skillful VOS observers. Paired OWS and VOS observations (near in space and coincident in time) were examined to see if there were consistent patterns relating a specific cloud type identified by OWS to that identified by VOS. The results were inconclusive, probably because most paired OWS and VOS observations were insufficiently close to exclude natural mesoscale variability in cloud type. Despite the occurrence of differences in cloud type identification between OWS and VOS, the physical consistency between expected atmospheric processes and the seasonal and geographical distributions of various low cloud types calculated from VOS observations demonstrates that VOS cloud type identification is sufficiently accurate to examine relationships between MBL processes and climate.

3. Geographical and seasonal distributions of low cloud types

a. Analysis description

Three basic parameters describing the variability of cloud types are frequency of occurrence (FQ), amount-when-present (AWP), and average cloud amount (AMT), where AMT = FQ × AWP. This paper focuses on FQ since that parameter best describes how often various MBL structures occur over the ocean. AWP of a given type is of secondary importance for diagnosing MBL processes, although AMT is very important for other studies involving the radiative effects of clouds. Most variations in AMT of a cloud type are due to FQ; AWP is more uniform around the globe. Therefore, AMT can be approximated as being linearly proportional to FQ with proportionality constant AWP. Table 2 shows the area-weighted average daytime AWP of all grid boxes with good data for the nine low cloud types; these values should be close to the global annual means. Approximate distributions of low cloud type AMT can be obtained by multiplying the distributions of low cloud type FQ presented in this paper by the values in Table 2. Due to a change in observing procedure in 1982 it was necessary to calculate FQ of low cloud types by a somewhat unconventional method to avoid introducing biases. Nonetheless, the formulas used are still exact and are described in the appendix.

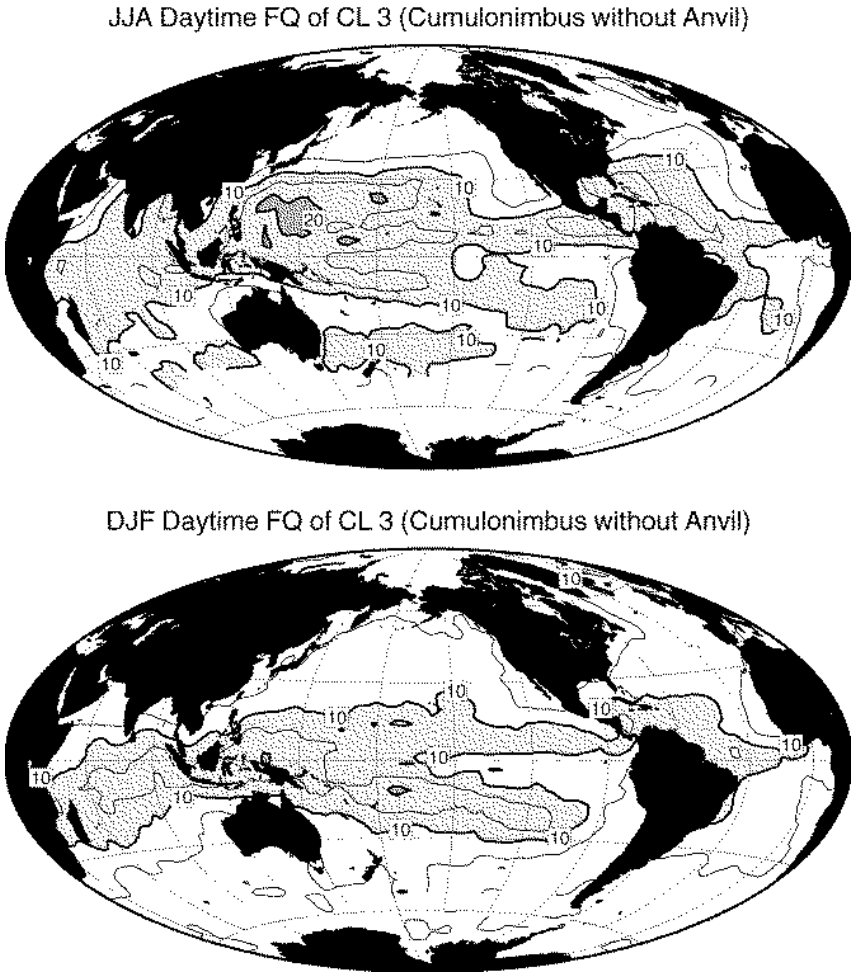

FIG. 3. Climatological JJA (top) and DJF (bottom) daytime FQ of C_L 3 (cumulonimbus-without-anvil). Contour interval is 5%. Shading indicates FQ above 10% (light) and 20% (dark).

Global climatologies of each low cloud type FQ were constructed by averaging surface observations from the time period 1954–92 in each box of the grids displayed in Fig. 2. Because the distribution of ships over the global ocean is highly nonuniform and large portions of the Tropics and Southern Hemisphere are poorly sampled, an irregular averaging grid was used to preserve resolution in regions with many observations and to increase statistical significance in regions with few observations. The base grid box size between 60°N and 60°S was 2.5° × 2.5° and increased in longitude poleward of 60° to preserve approximately equal areas. No grid box was more than four times the size of the base box for that latitude. Since OWS observers identify certain cloud types differently from VOS observers, all observations near OWS locations were excluded from the analysis. Grid boxes in well-sampled regions of the North Atlantic and North Pacific typically had several thousand observations contributing to the average, and grid boxes with less than 100 observations contributing to the average were discarded. After averaging, the value of each large grid box was assigned to all of the 2.5° × 2.5° base boxes within it and the resulting regular 2.5° × 2.5° grid was lightly smoothed prior to contouring. Contour intervals are different for various low cloud types but shading intervals are the same for all low cloud types to aid intercomparison. Values were calculated for each season, but only JJA and DJF maps are presented here.

The number of good nighttime observations is substantially less than the number of good daytime observations because surface observers sometimes have difficulty identifying low cloud type on nights with poor illumination (Rozendaal et al. 1995; Norris 1998). To avoid unevenly sampling the diurnal cycle only daytime and twilight observations were used, hereafter referred to as ''daytime'' [defined as when the sun is no more than 9° below the horizon, following the criterion of Hahn et al. (1995)]. The true diurnal average could be calculated by separately averaging daytime and nighttime values weighted by the length of day and night, but this would significantly decrease the statistical re-

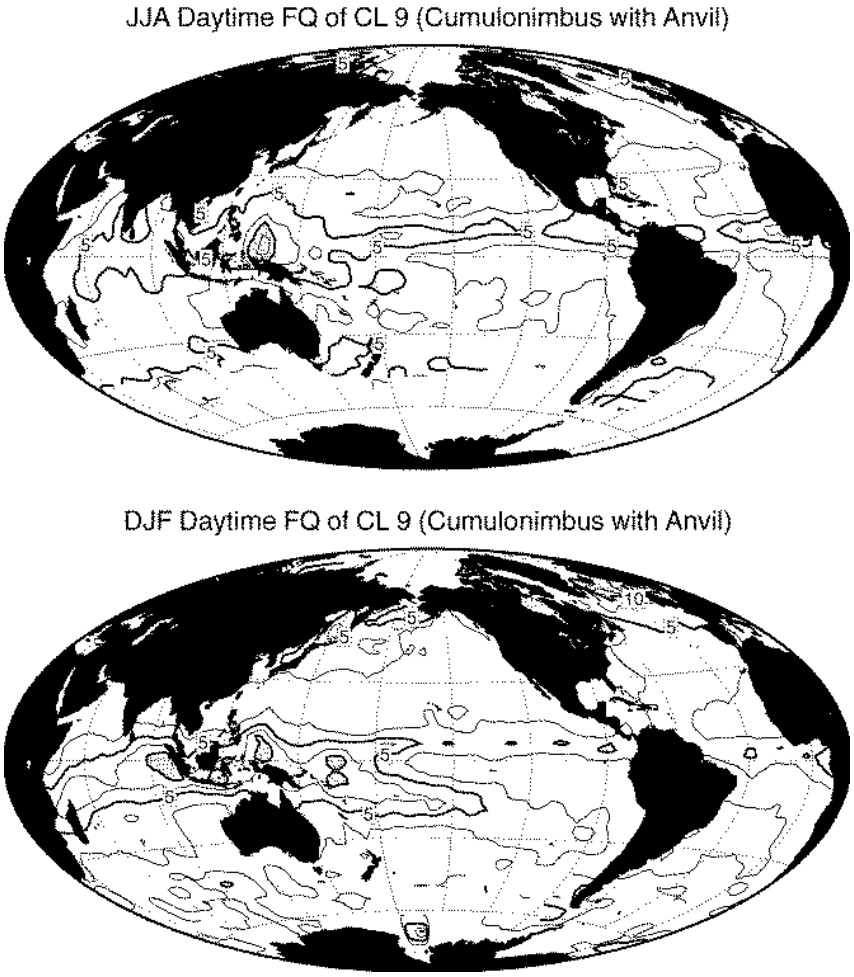

FIG. 4. Climatological JJA (top) and DJF (bottom) daytime FQ of C_L 9 (cumulonimbus-with-anvil). Contour interval is 2.5%. Shading indicates FQ above 10% (light) and 20% (dark).

liability of the results due to the smaller number of nighttime observations. Instead, only daytime values are presented (the W88 low cloud values were calculated from all observations). Since maxima and minima in cloudiness over the ocean typically occur in the early morning and afternoon and not at noon and midnight (Rozendaal et al. 1995), the daytime average may not actually differ greatly from the true diurnal average.

The data contoured in the following low cloud type climatologies may be obtained via FTP by contacting the author.

b. C_L 9 (cumulonimbus-with-anvil) and C_L 3 (cumulonimbus-without-anvil)

The W88 ''cumulonimbus'' category comprises C_L 3 (cumulonimbus-without-anvil) and C_L 9 (cumulonimbus-with-anvil) (Table 1), which are separately displayed in Fig. 3 (daytime FQ of C_L 3) and Fig. 4 (daytime FQ of C_L 9) for JJA and DJF. Regions of greatest cumulonimbus FQ coincide very well with regions of mean surface convergence in the Tropics and regions where the frequency of deep convection identified by the present-weather code reported by surface observers is also greatest (Petty 1995). The seasonal cycle and cumulonimbus FQ at low latitudes is consistent with the seasonal cycle of insolation.

However, distinct differences between the distributions of C_L 3 and C_L 9 are apparent. C_L 9 occurs only about half as frequently as C_L 3 over the ocean. This is in direct contrast to the situation over land where C_L 9 occurs much more frequently than C_L 3 (Hahn et al. 1988). Whereas C_L 9 sometimes occurs during winter east of the Eurasian coast and at high latitudes in the North Pacific and North Atlantic, probably as a result of cold air outbreaks, C_L 3 FQ over the ocean outside the Tropics is minimum along continental coasts. Unlike tropical maxima in C_L 3 FQ, tropical maxima in C_L 9 FQ usually occur close to land and coincide with regions of maximum SST, particularly over the maritime continent, the Caribbean, near the coast of Central America, and near the coast of Guinea. For all these regions sur-

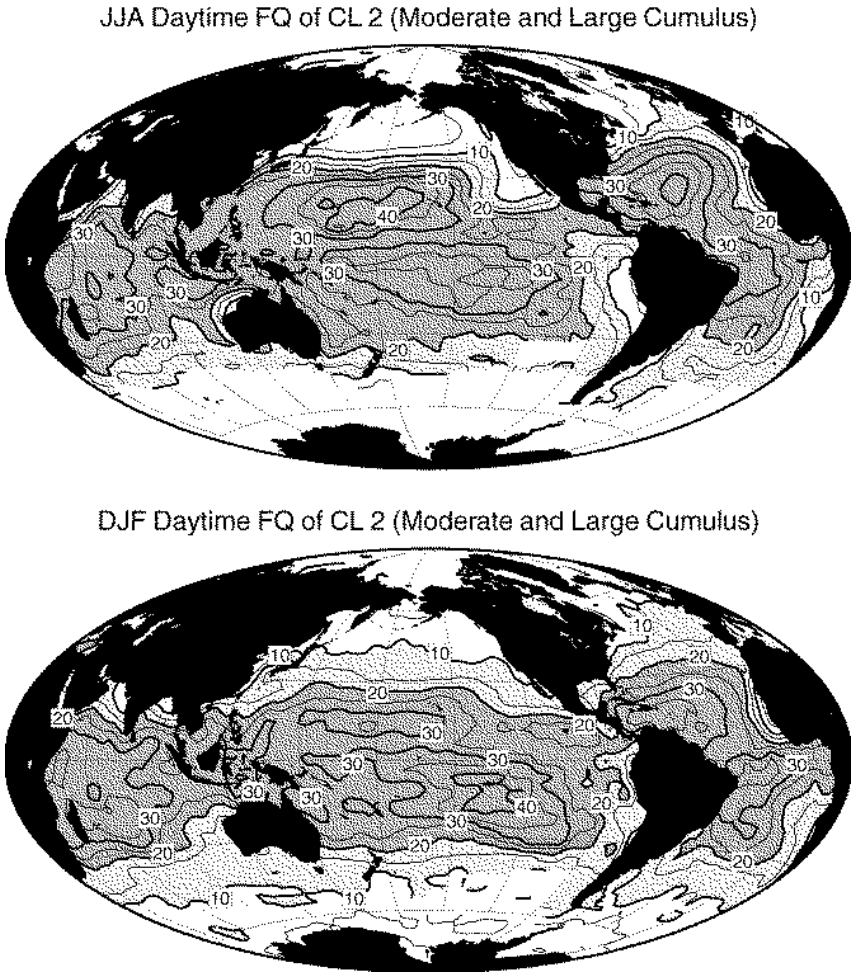

FIG. 5. Climatological JJA (top) and DJF (bottom) daytime FQ of C_L 2 (moderate and large cumulus). Contour interval is 5%. Shading indicates FQ above 10% (light) and 20% (dark).

face observers report a particularly high incidence of thunderstorm precipitation relative to all other nondrizzle precipitation (Petty 1995). This and the fact that lightning is also rare over most of the ocean except for these regions (Orville and Henderson 1986) suggests that C_L 9 is often associated with thunderstorm activity in the Tropics.

c. C_L 2 (moderate and large cumulus) and C_L 1 (small cumulus)

The W88 ''cumulus'' category comprises C_L 2 (moderate and large cumulus) and C_L 1 (small cumulus) (Table 1), which are separately displayed in Fig. 5 (daytime FQ of C_L 2) and Fig. 6 (daytime FQ of C_L 1) for JJA and DJF. Cumulus is very frequent in western and central tropical subtropical oceans and occurs slightly less frequently where cumulonimbus is most frequent. Because cumulonimbus has priority in designating the low cloud type code, it is possible that cumulus is actually no less frequent in the intertropical convergence zone (ITCZ) and corresponding regions than in the central subtropical oceans. Cumulus is rare at midlatitudes, especially during summer when warm advection prevails in the western North Pacific and North Atlantic (Klein and Hartmann 1993). This is consistent with the results of Part I, which implied that cumulus at midlatitudes is a cold-advection cloud type (Norris 1998). During summer more cold advection occurs in the eastern midlatitude North Pacific and North Atlantic than farther west and cumulus is relatively more frequent there.

Several differences between the distributions of C_L 2 and C_L 1 are apparent. C_L 1 is generally not as frequent as C_L 2, perhaps in part due to the fact that C_L 2 has priority over C_L 1 in designating the low cloud type code. Maximum C_L 1 FQ tends to occur along the fringes of regions of maximum C_L 2 FQ, especially in the western and central subtropical North Pacific during JJA. In central subtropical oceans in each hemisphere, C_L 2 FQ is generally minimum and C_L 1 FQ is generally maximum during the winter season. This is consistent with greater subsidence in the subtropics of the winter

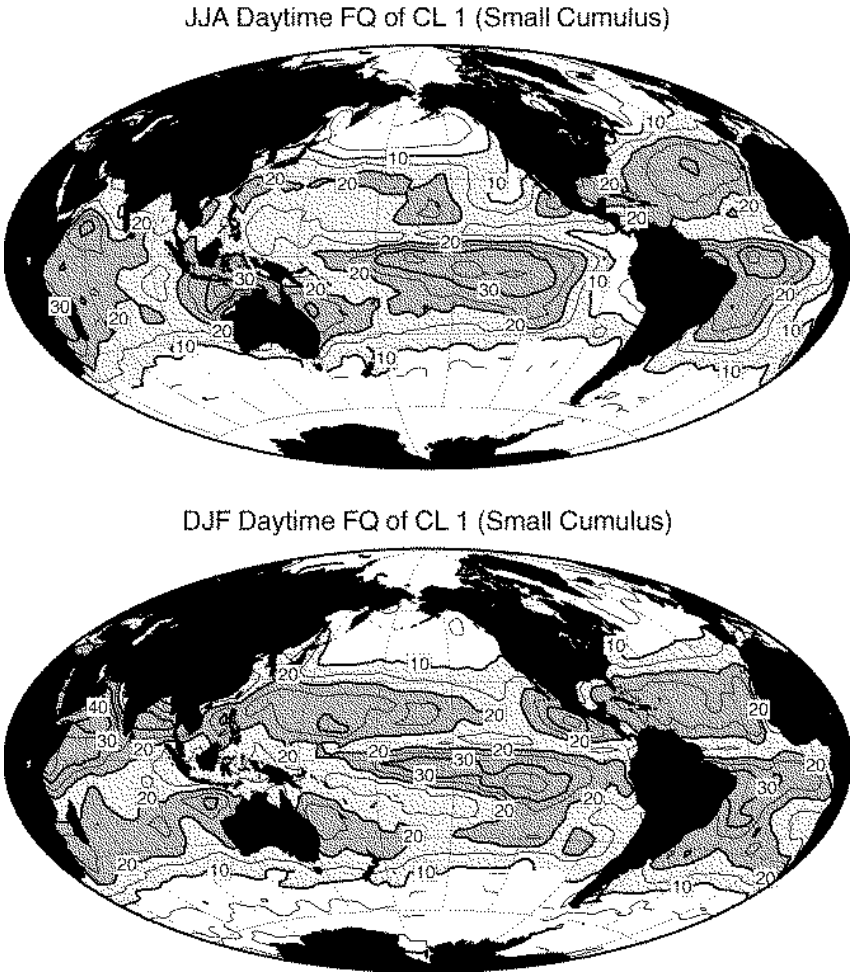

FIG. 6. Climatological JJA (top) and DJF (bottom) daytime FQ of C_L 1 (small cumulus). Contour interval is 5%. Shading indicates FQ above 10% (light) and 20% (dark).

hemisphere (Hoskins et al. 1989), which could promote a lower trade inversion that decreases the vertical extent of cumulus clouds and causes them to be identified as C_L 1 (small cumulus) more often. During winter at midlatitudes C_L 1 sometimes occurs along the eastern coasts of Eurasia and North America and is probably associated with cold-air outbreaks.

d. C_L 5 (ordinary stratocumulus) and C_L 6 (fair-weather stratus)

Klein and Hartmann (1993) documented that W88 ''stratus'' cloud amount was greatest over midlatitude and eastern subtropical oceans but could not distinguish the relative contributions of each stratus and stratocumulus cloud type that contributed to W88 stratus (Table 1). Figures 7 and 8 display the daytime FQ of C_L 5 (ordinary stratocumulus) and C_L 6 (fair-weather stratus), respectively, for JJA and DJF. Here we see that W88 stratus at midlatitudes is distinctly different from W88 stratus over the eastern subtropical ocean. C_L 5 is most common over eastern subtropical oceans but C_L 6 is most common at midlatitudes, particularly during summer, and rarely occurs over eastern subtropical oceans except near coastal upwelling regions.

These differences are generally consistent with the results of Part I, which indicated that C_L 6 at midlatitudes typically occurs in a relatively deep, stratified cloud layer with warm advection and weak synoptic ascent, whereas C_L 5 typically occurs in a shallow inversion-capped MBL with cold advection and subsidence. Warm advection and weak synoptic ascent occur most frequently over midlatitude oceans during summer, where C_L 6 is correspondingly most prevalent; warm advection is greatest (Klein and Hartmann 1993) and synoptic activity is weakest (Hoskins et al. 1989) over the North Pacific during summer, the region where C_L 6 is most common outside the Arctic. The frequent occurrence of C_L 6 over the Arctic Ocean during summer is consistent with the advection of warm air from the

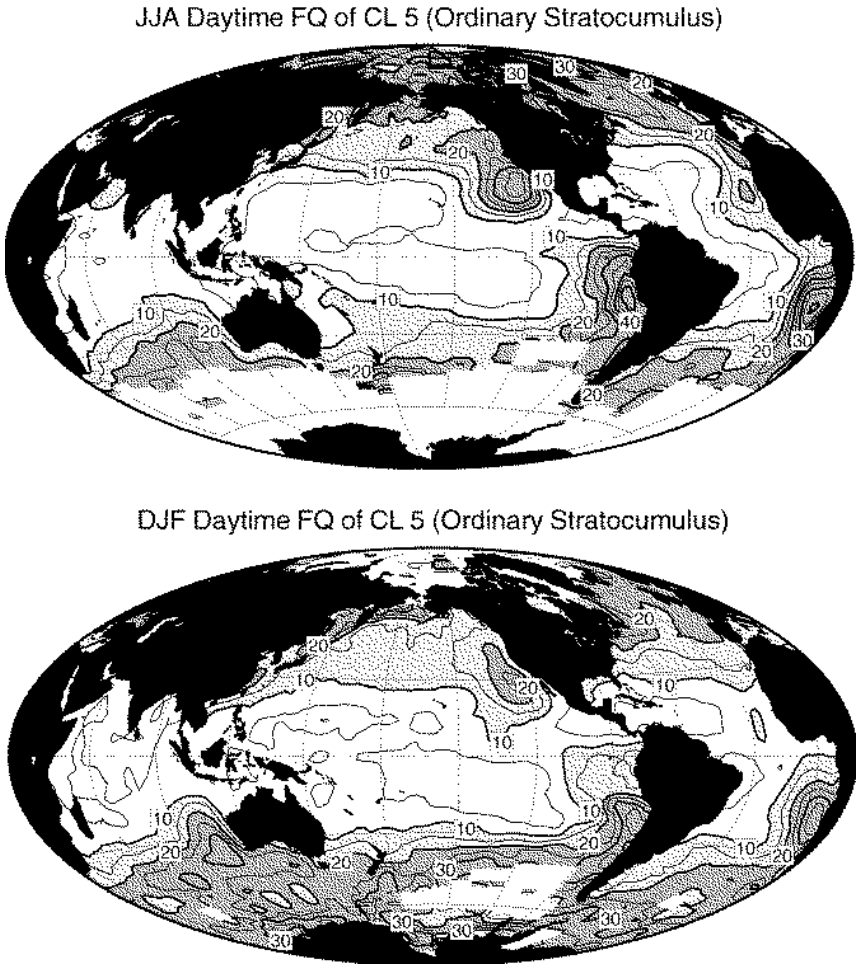

FIG. 7. Climatological JJA (top) and DJF (bottom) daytime FQ of C_L 5 (ordinary stratocumulus). Contour interval is 5%. Shading indicates FQ above 10% (light) and 20% (dark).

surrounding landmasses (Herman and Goody 1976). On the other hand, cold advection and subsidence occur most frequently over the eastern subtropical ocean where C_L 5 is correspondingly most common. During winter, stratocumulus is frequent east of the Eurasian and North American continents, probably as a result of cold-air outbreaks.

Soundings from coastal stations indicate that eastern subtropical stratus occurs in a very shallow mixed layer (Lilly 1968), unlike the case for midlatitudes (Norris 1998). Cloudiness occurring in well-mixed MBLs probably has less horizontal inhomogeneity than cloudiness occurring in less well-mixed MBLs, prompting observers to identify it as C_L 6 instead of C_L 5. The area of C_L 6 next to the California coast roughly corresponds to the area where Bretherton and Wyant (1997) predict a coupled cloud-topped MBL. Observations from the Arctic indicate that summertime stratus also typically occurs in a relatively shallow boundary layer, sometimes in multiple cloud decks (Curry et al. 1988).

e. C_L 8 (cumulus-under-stratocumulus[1]) and C_L 4 (stratocumulus-from-spreading-cumulus)

C_L 8 (cumulus-under-stratocumulus) and C_L 4 (stratocumulus-from-spreading-cumulus) are two additional cloud types that contribute to W88 stratus (Table 1). Both are composed of cumulus with stratocumulus and are distinguished from each other by whether the cumulus clouds widen as they reach the stratocumulus layer (WMO 1975), the case for C_L 4. Otherwise cumulus with stratocumulus is identified as C_L 8. This appears to be a subtle difference in practice, however, and the fact that OWS observers almost never report C_L 4 (Fig. 1) suggests that VOS observers often report as C_L 4 what better-trained OWS observers would report

[1] The WMO description of C_L 8 merely states ''the base of the cumulus is at a different level than that of the stratocumulus'' (Table 1 in Part I), but cumulus-under-stratocumulus is an appropriate paraphrase because stratocumulus-under-cumulus is unphysical.

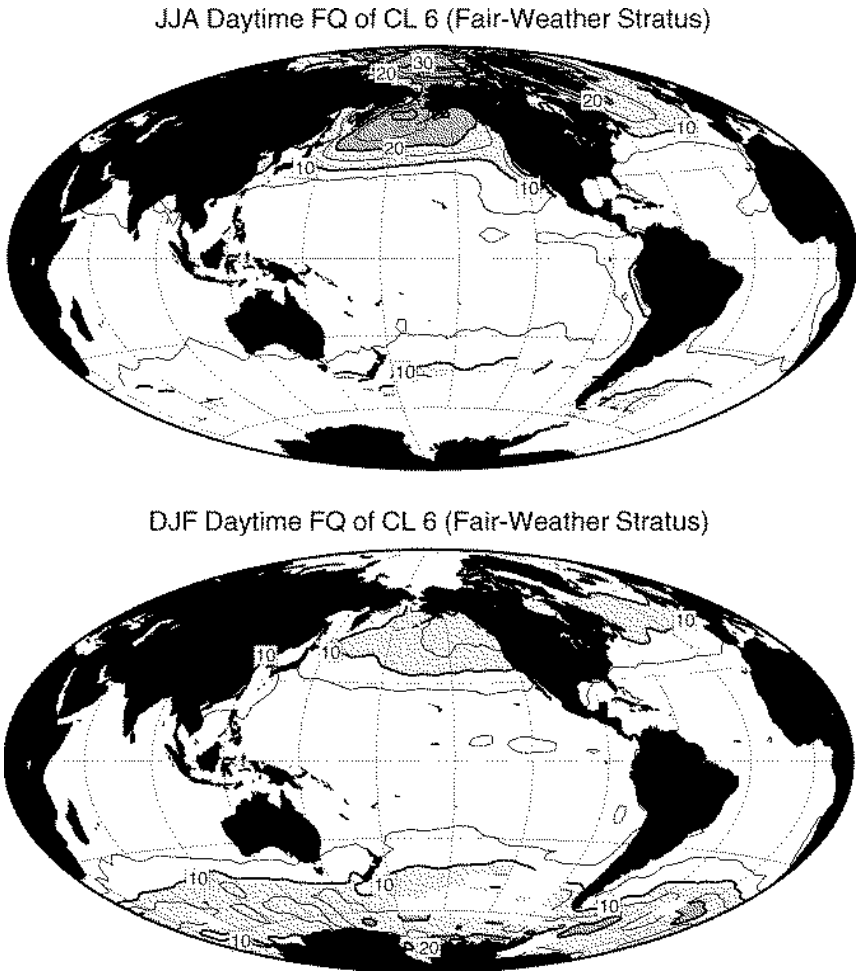

FIG. 8. Climatological JJA (top) and DJF (bottom) daytime FQ of C_L 6 (fair-weather stratus). Contour interval is 5%. Shading indicates FQ above 10% (light) and 20% (dark).

as C_L 8. This is confirmed by the great similarity between the geographical and seasonal distributions of daytime FQ of C_L 8 (Fig. 9) and that of C_L 4 (Fig. 10). For this reason it is assumed that VOS observations of C_L 4 and C_L 8 generally correspond to the same cumulus-with-stratocumulus cloud type, MBL structure, and meteorological conditions associated with OWS observations of C_L 8 in Part I (Norris 1998).

Similar to ordinary stratocumulus, cumulus-with-stratocumulus typically occurs in an inversion-capped MBL with cold advection and subsidence (Norris 1998) and is correspondingly frequent where ordinary stratocumulus is frequent. However, a comparison of Figs. 9 and 10 with Figs. 7 and 5 shows that the geographical location of maximum cumulus-with-stratocumulus FQ occurs between maximum ordinary stratocumulus FQ and maximum ordinary cumulus FQ. This is consistent with the conceptual model of Bretherton (1992) and Wyant et al. (1997), which proposes a transition in MBL cloudiness from ordinary stratocumulus to cumulus-under-stratocumulus to ordinary cumulus as the MBL is advected by trade winds over increasingly warm SST (discussed in more detail in section 4a). A similar transition also occurs north of the equatorial cold tongue in the eastern tropical Pacific (discussed in more detail in section 4b).

f. C_L 7 (bad-weather stratus) and sky-obscuring precipitation

Figure 11 displays the JJA and DJF climatological distributions of daytime FQ of C_L 7 (bad-weather stratus), which also contributes to W88 stratus (Table 1). Part I of this study documented that at midlatitudes this cloud type is associated with nearly saturated conditions through the middle and lower troposphere and usually occurs with rain (Norris 1998). Correspondingly, C_L 7 is most frequent at midlatitudes during winter when synoptic activity is greatest. The relatively weak but well-defined storm track of C_L 7 stretching across the midlatitude North Pacific during JJA is consistent with relatively weak synoptic activity indicated by high-pass-

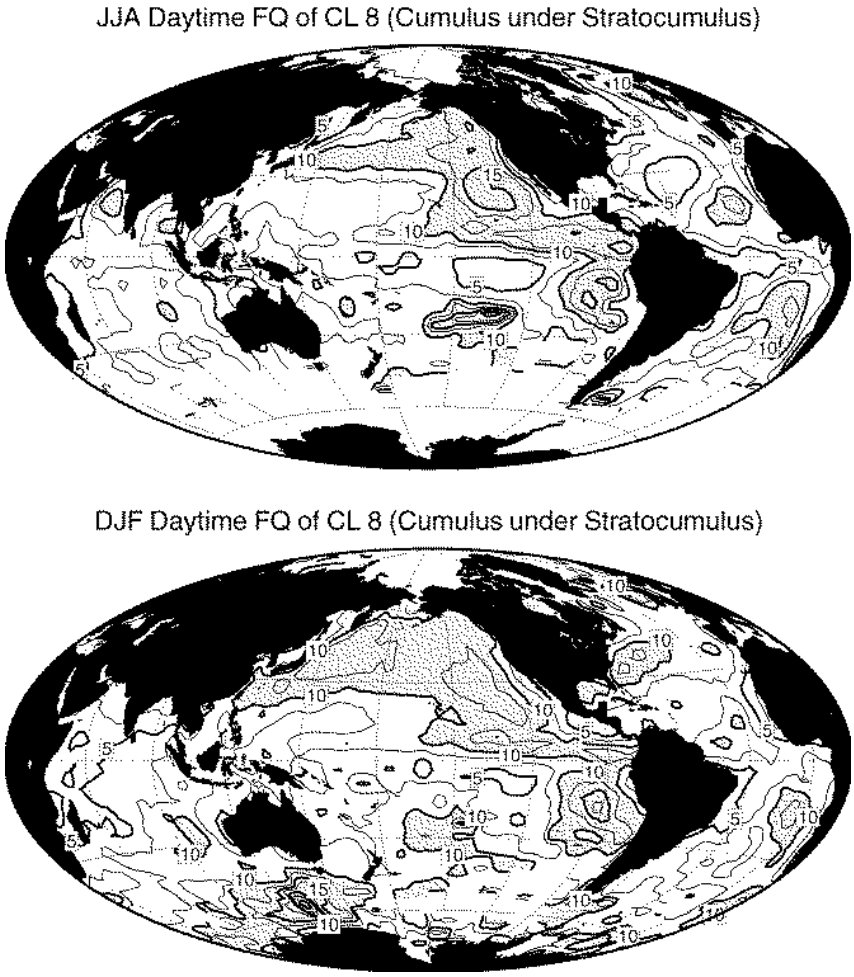

FIG. 9. Climatological JJA (top) and DJF (bottom) daytime FQ of C_L 8 (cumulus-under-stratocumulus). Contour interval is 2.5%. Shading indicates FQ above 10% (light) and 20% (dark).

filtered 250-mb wind statistics and coincides with a band of mean upward motion in the midtroposphere (Hoskins et al. 1989). At lower latitudes C_L 7 is probably associated with stratiform precipitation regions of mesoscale convective systems (Houze 1993).

Sky-obscuring precipitation is diagnosed when the total cloud cover code reports sky-obscured (N = 9) and the present-weather code (ww) reports precipitation, usually drizzle or snow, at the time and location of the observation (ww = 50–75, 77, 79, 80–99). Figure 12 displays JJA and DJF climatological distributions of daytime FQ of sky-obscuring precipitation. Sky-obscuring precipitation is negligible over most of the ocean but occasionally occurs at midlatitudes. During summer a much larger fraction of precipitation occurs as drizzle in the North Pacific compared to the North Atlantic (Petty 1995), which is consistent with the much greater FQ of sky-obscuring precipitation in the North Pacific. The fact that the geographical distributions of sky-obscuring precipitation and sky-obscuring fog (Fig. 13) are similar during summer suggests that reports of sky-obscuring precipitation due to drizzle actually result from sky-obscuring fog with coincident drizzle. The present-weather code requires the largest applicable number to be reported, so drizzle (ww = 50–59) has priority over fog (ww = 10–12, 40–49). During winter most precipitation in the western North Pacific and western North Atlantic occurs as snow (Petty 1995), which is consistent with the greater FQ of sky-obscuring precipitation in these regions.

g. Sky-obscuring fog and C_L 0 (no-low-cloud)

Figure 13 displays the JJA and DJF climatological distributions of daytime FQ of sky-obscuring fog, which also contributes to W88 stratus. These maps are basically higher-resolution versions of maps 100 and 102 previously calculated by Warren et al. (1988). Sky-obscuring fog is rare over most of the ocean except in the western midlatitude North Pacific and North Atlantic

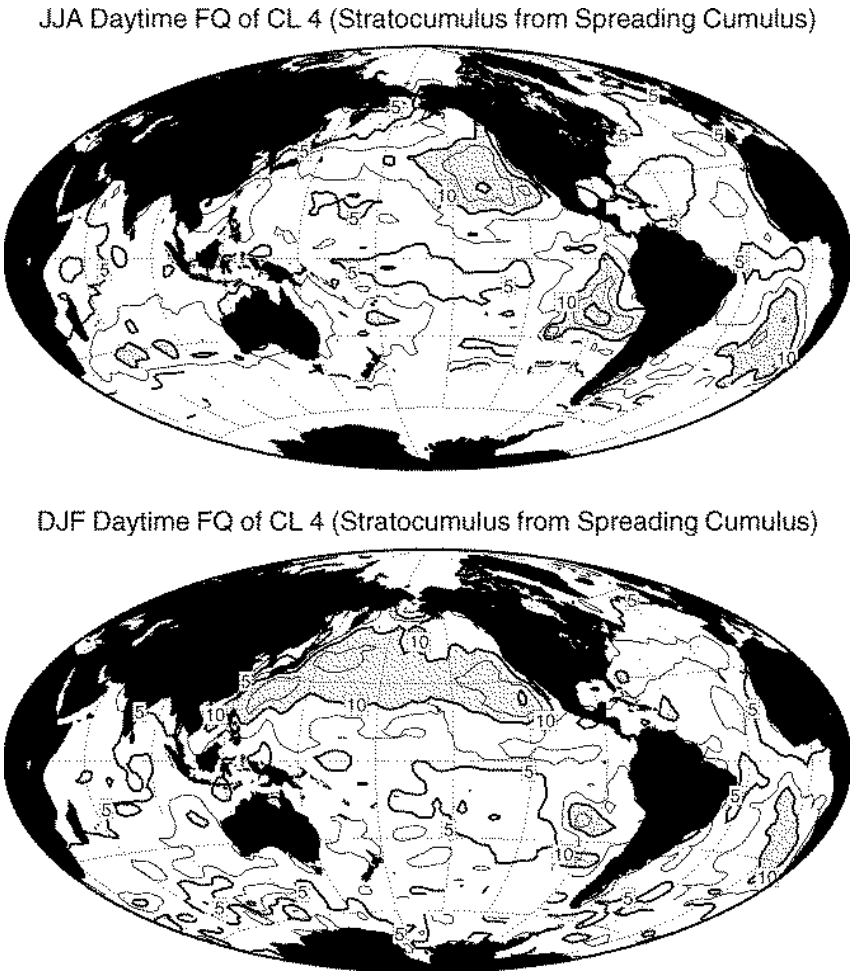

FIG. 10. Climatological JJA (top) and DJF (bottom) daytime FQ of C_L 4 (stratocumulus-from-spreading-cumulus). Contour interval is 2.5%. Shading indicates FQ above 10% (light) and 20% (dark).

and parts of the Arctic during summer where substantial warm advection occurs (Klein and Hartmann 1993). The maximum FQ of sky-obscuring fog occurs where mean warm advection (including eddy terms) is greatest (not shown). This is consistent with Part I of this study, which showed that sky-obscuring fog is associated with strong warm advection (Norris 1998). Some sky-obscuring fog also occurs in the Southern Ocean during summer.

Figure 14 displays the JJA and DJF climatological distributions of daytime FQ of C_L 0 (no-low-cloud). C_L 0 is very frequent adjacent to continents, over the Mediterranean Sea, and over the Arctic Ocean, and sometimes occurs poleward and eastward of continents at midlatitudes during summer, where poleward and eastward is usually downwind. This in combination of results from Part I for OWS B and C in the western North Atlantic (Norris 1998) suggests that C_L 0 is associated with warm advection of dry air from land. C_L 0 also sometimes occurs on the southern side of the equatorial cold tongue in the Pacific and Atlantic Oceans where southerly winds advect air over colder SST. Here it is likely that the increased stratification sometimes reduces entrainment-generating turbulence to the point that subsidence pushes the base of the trade inversion beneath the lifting condensation level or reduces upward moisture flux to the point that the cloud layer evaporates (described in further detail in section 4b). Cloudless MBLs are correspondingly more frequent during JJA when the equatorial cold tongue and surface divergence are stronger. A similar process may occur around 30°N during DJF in a zone of surface divergence between the subtropics and midlatitudes (not shown).

4. Transitions in cloud type

a. Eastern subtropical ocean

The stratocumulus to trade cumulus transition in the eastern subtropical ocean is explored in greater detail

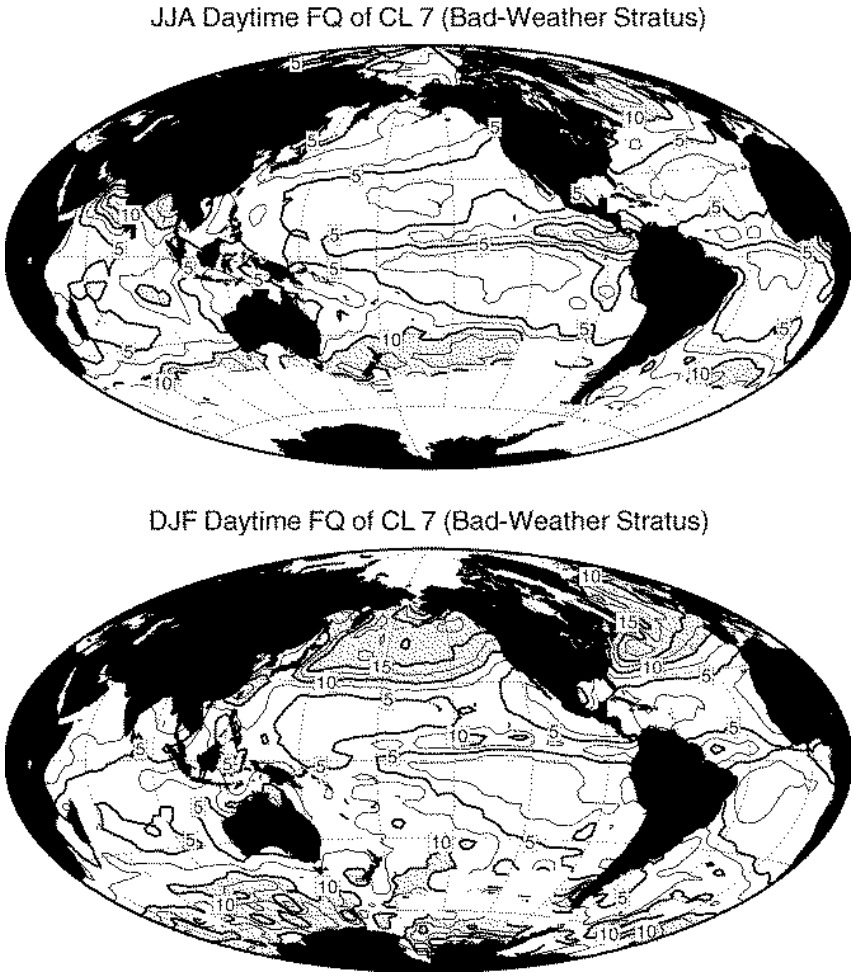

FIG. 11. Climatological JJA (top) and DJF (bottom) daytime FQ of C_L 7 (bad-weather stratus). Contour interval is 2.5%. Shading indicates FQ above 10% (light) and 20% (dark).

by calculating climatological values of MBL properties and daytime FQ of cloud types along a trajectory around the subtropical anticyclone during JJA. The trajectory is chosen to pass through the location of maximum stratocumulus FQ and the averaging regions are spaced one day apart at the climatological surface wind speed following the climatological surface wind direction (indicated in Fig. 15). This should be representative of typical synoptic trajectories since the trade winds are particularly steady during summer. Figure 16a shows a consistent progression in the locations of maximum FQ of fair-weather stratus (C_L 6), ordinary stratocumulus (C_L 5), cumulus-with-stratocumulus FQ (C_L 8 and 4), cumulus (C_L 1 and 2), and cumulonimbus (C_L 3 and 9) as the climatological MBL is advected equatorward into the ITCZ. The cumulus category is dominated by small cumulus (C_L 1) upstream and moderate and large cumulus (C_L 2) downstream (not shown).

Climatological along-trajectory variations of SST, nighttime air–sea temperature difference ($\Delta T \equiv T_{air} -$ SST), surface divergence, and inversion base height during JJA show that the observed transition in cloud type is consistent with the conceptual model of Bretherton (1992) and Wyant et al. (1997). Here, ΔT was calculated using only nighttime observations to avoid biases resulting from ship deck heating (Goerss and Duchon 1980). Surface divergence was calculated from surface-observed winds, and inversion base heights were obtained from the climatology of Neiburger et al. (1961). Figure 16b shows that SST steadily increases as the MBL is advected toward the equator. Surface air temperature increases as well, though not as much, which results in an increasingly negative ΔT (Fig. 16b). Both of these contribute to an increasingly large moisture flux into the MBL, which Wyant et al. suggest is responsible for the decoupling of the cloud layer from the subcloud layer. Figure 16c shows that surface divergence is greatest near the beginning of the trajectory and decreases farther downstream to eventually become net convergence in the ITCZ. Mixed-layer modeling (Schubert et al. 1979) and observations following a synoptic trajectory (Bretherton and Pincus 1995; Bretherton et al.

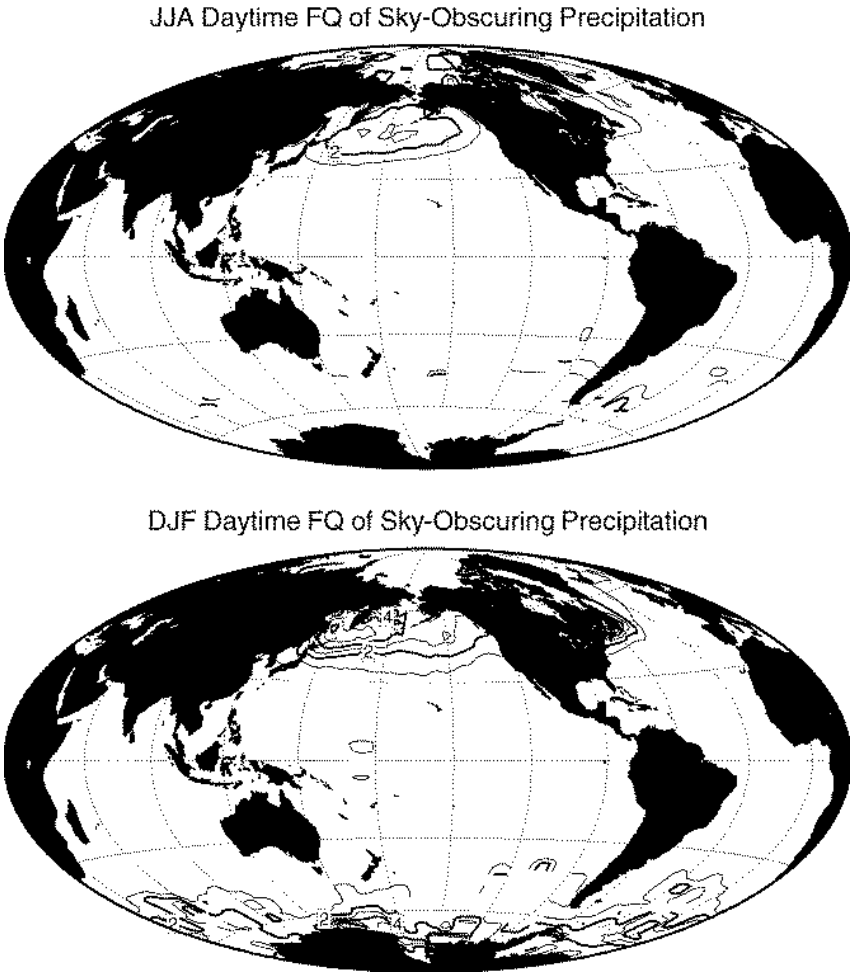

FIG. 12. Climatological JJA (top) and DJF (bottom) daytime FQ of sky-obscuring precipitation. Contour interval is 1%. Shading indicates FQ above 10% (light) and 20% (dark).

1995) indicate decreasing surface divergence and increasing SST both contribute to the observed deepening of the MBL (Fig. 16c). Increasing MBL depth also promotes decoupling (Wyant et al. 1997), and increasing decoupling promotes the transition in low cloud type from ordinary stratocumulus to cumulus-with-stratocumulus to ordinary cumulus. This is consistent with the results of Part I, which showed that at specific locations the MBL is typically shallowest for stratocumulus, deepest for cumulus, and in-between for cumulus-with-stratocumulus (Norris 1998).

b. Eastern equatorial ocean

MBLs advected northward from the eastern subtropical South Pacific pass over the equatorial cold tongue prior to entering the ITCZ, resulting in a rapid transition from advection over colder SST to advection over much warmer SST and a correspondingly rapid transition in cloud type (Figs. 17a and 17c). This transition is examined in a region of the eastern equatorial Pacific (indicated in Fig. 15) through the use of zonal averages instead of a trajectory in order to compensate for the lower sampling density. This should not greatly affect the results because MBL properties and cloud type FQ and are generally zonally uniform within the region. Climatological values of MBL properties and daytime FQ of cloud types are calculated for JJA, a season when the meridional SST gradient and meridional wind are particularly strong (Mitchell and Wallace 1992). Similar to Fig. 7b of Klein and Hartmann (1993), Fig. 17b shows the rapid decrease and even more rapid increase in SST that occurs during advection over the cold tongue. Advection over colder SST south of the minimum SST causes the nighttime ΔT to become much less negative, almost to the point of zero (Fig. 17b). Advection over warmer SST north of the minimum SST dramatically reverses this, and ΔT becomes strongly negative in about one day. Net surface divergence occurs over and south of the cold tongue and becomes net convergence in the

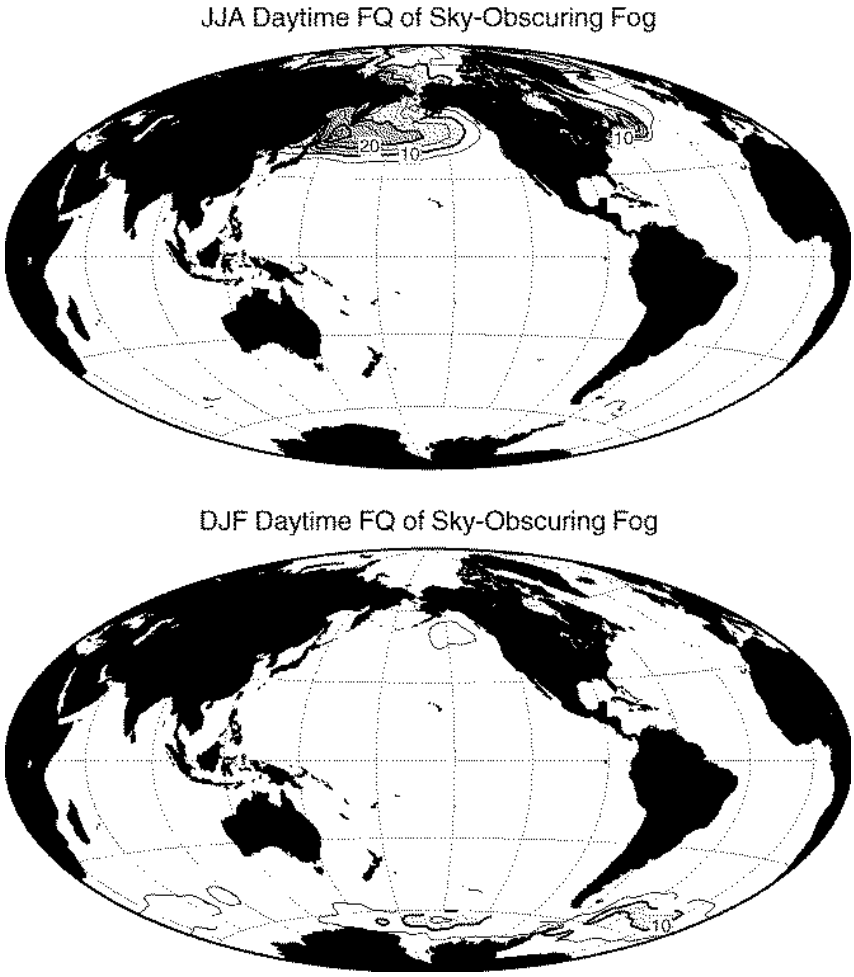

FIG. 13. Climatological JJA (top) and DJF (bottom) daytime FQ of sky-obscuring fog. Contour interval is 5%. Shading indicates FQ above 10% (light) and 20% (dark).

ITCZ (Klein and Hartmann 1993). However, the large increase in surface divergence over the northern side of the cold tongue observed by Klein and Hartmann probably does not reflect a large increase in subsidence but instead results from enhanced downward momentum flux as the MBL goes from positively to negatively stratified (Wallace et al. 1989).

Figures 17a and 17c show that the observed cloud type transition is consistent with the latitudinal variation of advection and surface divergence. As is the case north of the ITCZ, cumulus is the most frequent cloud type south of the cold tongue. Small cumulus (C_L 1) becomes relatively more prevalent than large cumulus (C_L 2) over the southern side of the cold tongue, consistent with the shallower MBL observed south of the Equator (Haraguchi 1968) resulting from advection over decreasing SST (Schubert et al. 1979). No-low-cloud (C_L 0) has maximum FQ over the cold tongue, one of the few places over the global ocean away from land where it occurs with any frequency (Fig. 14). The MBL is positively stratified on the southern side of the cold tongue (Bond 1992), which reduces upward moisture fluxes and entrainment-generating turbulence. It is possible that cloudless MBLs result from occasional conditions of particularly strong subsidence and MBL stratification that cause the lifting condensation level to descend beneath the inversion base; observations by Neiburger et al. (1961) indicate that inversion base over the cold tongue during JJA is sometimes lower than 600 m. Alternately, strong stratification may reduce the upward moisture flux to the point that the cloud layer evaporates. North of the minimum SST, surface divergence and advection over much warmer SST generate increased stratocumulus (C_L 5), as previously documented by Deser et al. (1993). The maximum FQ of cumulus-with-stratocumulus (C_L 8 and 4) occurs downstream from the maximum FQ of stratocumulus, as is the case in the eastern subtropical ocean. The FQ of small cumulus and stratocumulus decreases and the FQ of large cumulus, cumulonimbus (C_L 3 and 9), and bad-weather stratus (C_L 7) increases when surface divergence reverses to convergence as the MBL approaches the ITCZ.

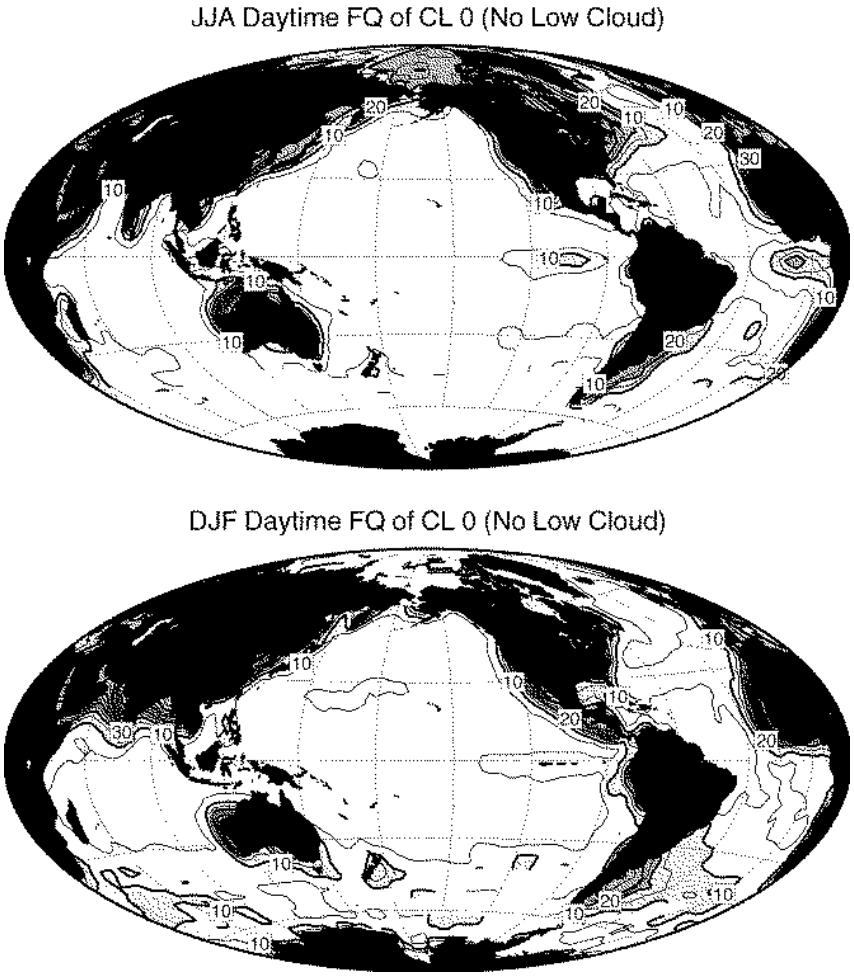

FIG. 14. Climatological JJA (top) and DJF (bottom) daytime FQ of C_L 0 (no-low-cloud). Contour interval is 5%. Shading indicates FQ above 10% (light) and 20% (dark).

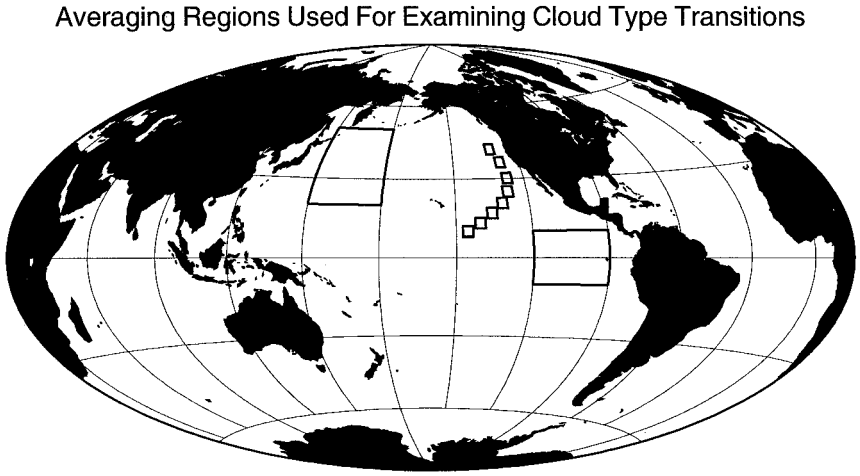

FIG. 15. Averaging regions used for examining low cloud type transitions.

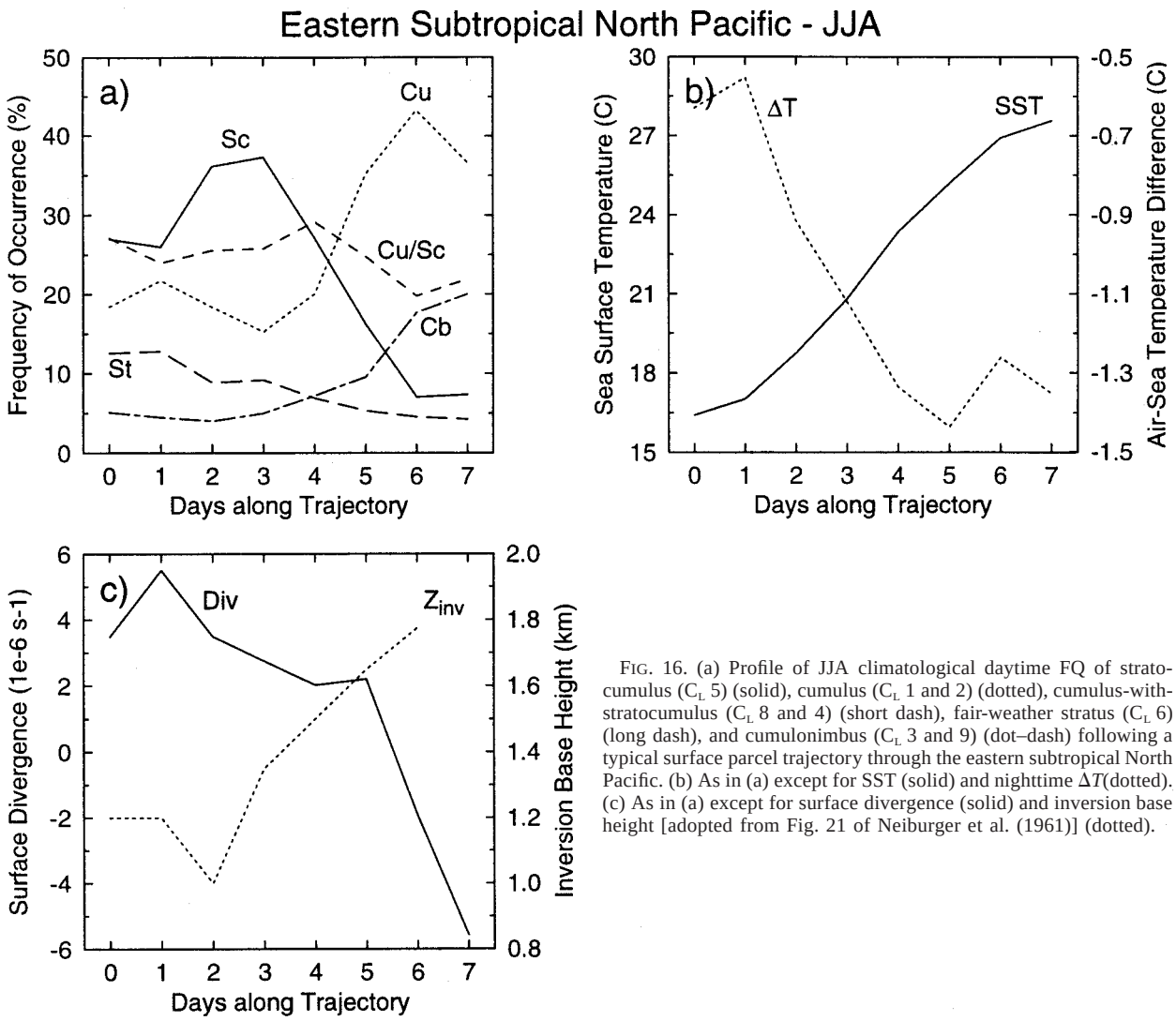

FIG. 16. (a) Profile of JJA climatological daytime FQ of stratocumulus (C_L 5) (solid), cumulus (C_L 1 and 2) (dotted), cumulus-with-stratocumulus (C_L 8 and 4) (short dash), fair-weather stratus (C_L 6) (long dash), and cumulonimbus (C_L 3 and 9) (dot–dash) following a typical surface parcel trajectory through the eastern subtropical North Pacific. (b) As in (a) except for SST (solid) and nighttime ΔT(dotted). (c) As in (a) except for surface divergence (solid) and inversion base height [adopted from Fig. 21 of Neiburger et al. (1961)] (dotted).

c. Western subtropical/midlatitude ocean

Although much recent research on the role of MBL cloudiness in the climate-system has focused on eastern subtropical stratocumulus, Norris and Leovy (1994) documented that substantial interannual variability in stratiform cloudiness and SST occurs in the western and central North Pacific and North Atlantic during summer. Much of this variability was attributed to year-to-year latitudinal shifts in the location of the storm track and regions of strong SST and cloudiness gradients. To examine the relationship between cloudiness and SST in greater detail, climatological values of both are calculated during JJA for a region in the western North Pacific (indicated in Fig. 15). Climatological values during JJA for a region in the western North Atlantic (not shown) are similar. Figures 18a and 18c show the latitudinal variation of daytime FQ of various cloud types and Fig. 18b shows the latitudinal variation of SST and nighttime ΔT. Generally, southerly surface winds over northward decreasing SST produce seasonal mean warm advection in this region, and climatological ΔT goes from negative to positive between the subtropics and midlatitudes and has latitudinal variation very similar to that of seasonal mean daily temperature advection at 1000 mb (not shown). However, persistent warm advection rarely occurs due to frequent synoptic activity, which can cause southward flow as well as northward flow over the SST gradient.

Southward flow over the SST gradient produces cold advection similar to that previously examined in the eastern subtropical North Pacific and eastern tropical Pacific north of the equatorial cold tongue. Figures 18a and 18c show a progression in the locations of maximum FQ of ordinary stratocumulus (C_L 5), cumulus-with-stratocumulus FQ (C_L 8 and 4), and cumulus (C_L 1 and 2) from north to south. This is consistent an increasingly

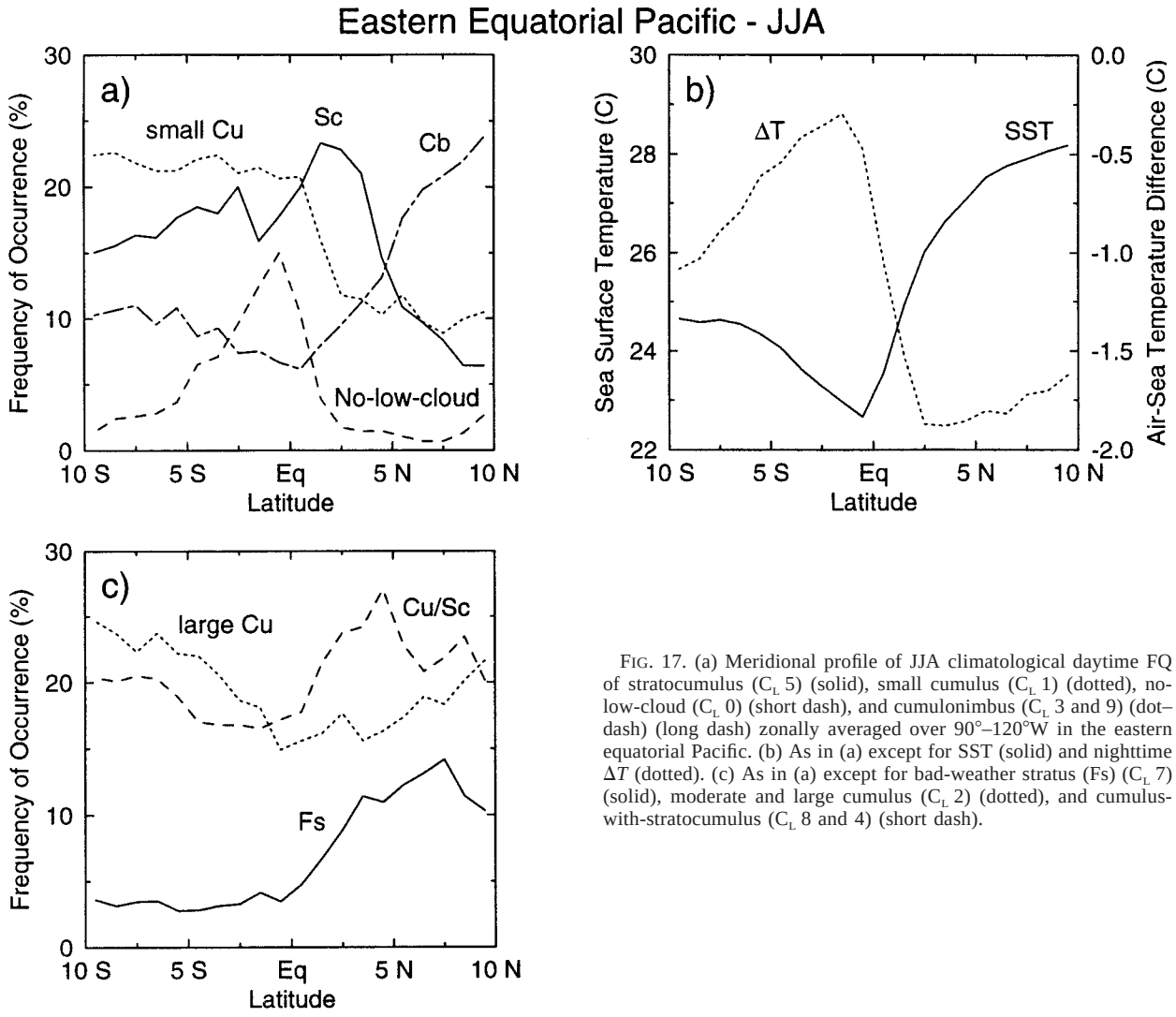

FIG. 17. (a) Meridional profile of JJA climatological daytime FQ of stratocumulus (C_L 5) (solid), small cumulus (C_L 1) (dotted), no-low-cloud (C_L 0) (short dash), and cumulonimbus (C_L 3 and 9) (dot–dash) (long dash) zonally averaged over 90°–120°W in the eastern equatorial Pacific. (b) As in (a) except for SST (solid) and nighttime ΔT (dotted). (c) As in (a) except for bad-weather stratus (Fs) (C_L 7) (solid), moderate and large cumulus (C_L 2) (dotted), and cumulus-with-stratocumulus (C_L 8 and 4) (short dash).

decoupled MBL resulting from advection over rapidly increasing SST.

Northward flow over rapidly decreasing SST increases the stratification of the surface layer and decreases convective available potential energy (CAPE), consistent with the poleward decrease in cumuliform cloud types. Small cumulus (C_L 1) has a maximum around 30°N and is slightly more frequent than moderate and large cumulus (C_L 2) at midlatitudes. Decreasing CAPE and increasing stratification will decrease the maximum height attained by cumulus and increase the probability that cumulus clouds will be identified as ''small'' instead of ''moderate or large.'' Composite soundings from Part I (Norris 1998) suggest that advection over colder SST can transform a MBL with cumulus to one with shallow fair-weather stratus (C_L 6), consistent with the poleward increase in fair-weather stratus. It is likely that further advection of this shallow stratus layer farther to the north will produce sky-obscuring fog under conditions of subsidence or a deeper stratus layer (as was observed at OWS C in Part I) under conditions of weak ascent. Bad-weather stratus (C_L 7) is produced by stronger ascent and has maximum FQ around 37.5°N, slightly south of the region of strongest SST gradient and coinciding with a band of mean upward motion in the midtroposphere (Hoskins et al. 1989).

5. Conclusions

Part I of this paper (Norris 1998) showed that surface-observed low cloud type was consistently related to the vertical distribution of temperature and moisture and surface meteorology at several OWS. Part II shows a similar consistency between geographical and seasonal distributions of low cloud type and expected patterns of advection, surface divergence, and synoptic activity over the global ocean. Detailed examinations of low cloud type variations along climatological trajectories

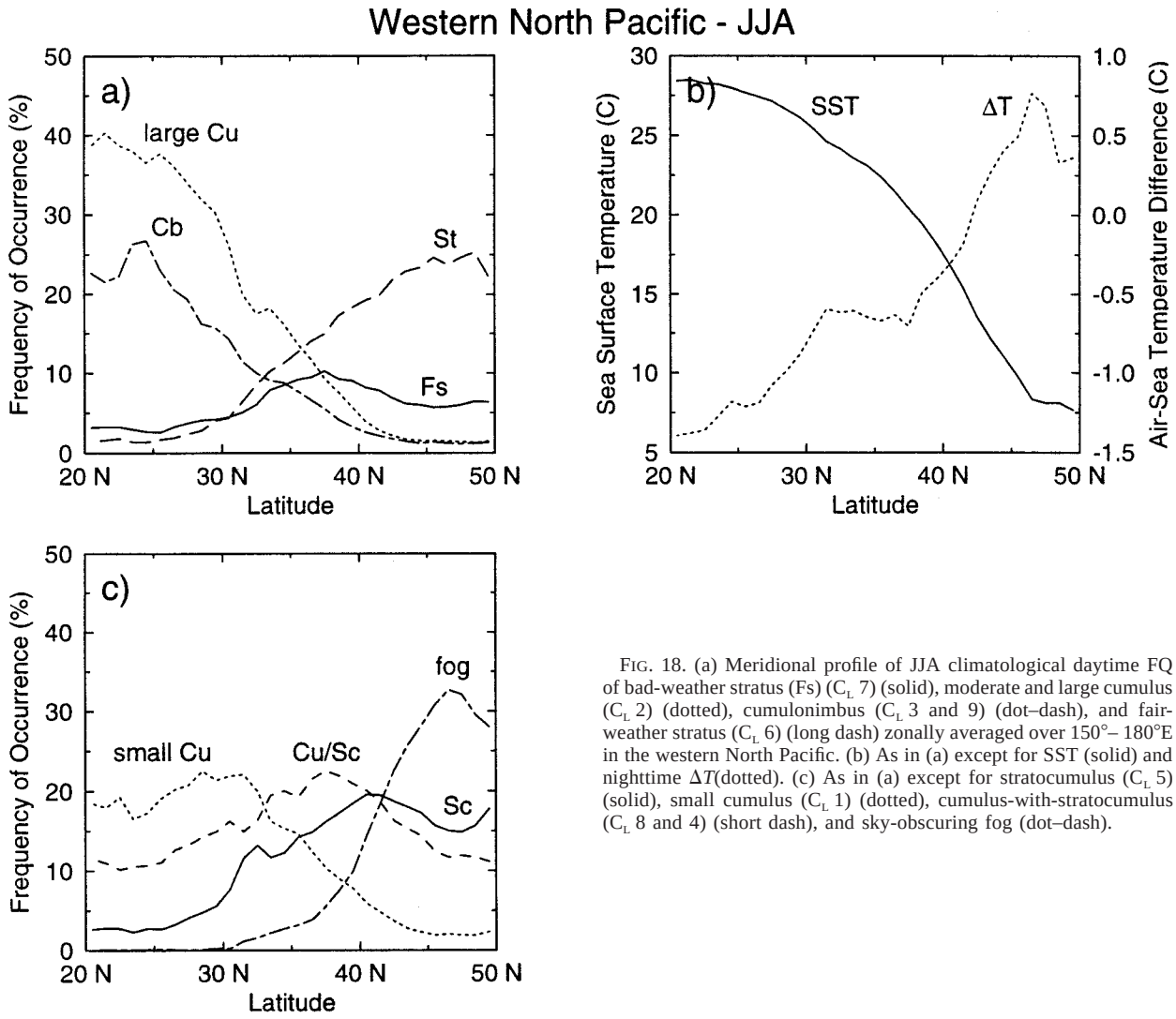

FIG. 18. (a) Meridional profile of JJA climatological daytime FQ of bad-weather stratus (Fs) (C_L 7) (solid), moderate and large cumulus (C_L 2) (dotted), cumulonimbus (C_L 3 and 9) (dot–dash), and fair-weather stratus (C_L 6) (long dash) zonally averaged over 150°– 180°E in the western North Pacific. (b) As in (a) except for SST (solid) and nighttime ΔT(dotted). (c) As in (a) except for stratocumulus (C_L 5) (solid), small cumulus (C_L 1) (dotted), cumulus-with-stratocumulus (C_L 8 and 4) (short dash), and sky-obscuring fog (dot–dash).

in the eastern subtropical North Pacific, eastern equatorial Pacific, and western North Pacific show that maxima in the frequency of stratocumulus, cumulus-with-stratocumulus, and cumulus progressively occur as the MBL is advected over increasingly warm SST. This transition is consistent with increased MBL height, increased decoupling of the cloud layer from the subcloud layer, and decreased surface divergence. Advection over increasingly cold SST sometimes produces a cloudless MBL on the southern side of the equatorial cold tongue and stratus or fog in the western midlatitude North Pacific.

These results suggest surface observations of low cloud type made by VOS can be used to qualitatively infer MBL structure where above-surface measurements are lacking. This will help elucidate processes responsible for variability in cloudiness over the ocean. Global climatologies of low cloud type can also provide a baseline for the development and validation of MBL cloud parameterizations in general circulation models. For example, the prevalence of cumulus-with-stratocumulus over the midlatitude ocean suggests the MBL is frequently decoupled there. Further investigation of interannual variability in low cloud type and related processes will provide better understanding of the role of MBL cloudiness over the ocean in the climate system.

Acknowledgments. This work was supported by an Earth Observing System grant, NASA Grant NAGW-2633, and in part by a NASA Global Change Fellowship, NASA Grant NGT-30092. Carole Hahn graciously provided the programs and computer resources to process the surface cloud observations. Stephen Klein substantially contributed to the OWS–VOS comparisons and provided the temperature advection data. The author wishes to thank Conway Leovy for his encouragement and support for this project and Stephen Klein, Stephen

Warren, Robert Houze, Marcia Baker, and an anonymous reviewer for their useful comments.

APPENDIX

Calculation of Low Cloud Type Frequency

As described in Hahn et al. (1994), a small fraction of ships report total cloud cover (N) but not low, middle, and high cloud types (C_L, C_M, and C_H). Prior to 1982 these reports could be excluded from calculations of the frequency of occurrence of low cloud types since C_L was recorded as ''/'' (no low cloud type information). However, a change in observing procedure in 1982 allowed observers to report C_L as ''/'' for conditions of clear skies (N = 0). Consequently, it was no longer possible to distinguish between ships that normally reported cloud type and those that did not. Ships that did not normally report cloud type would contribute to the frequency of clear sky but not to the frequency of cloud types, thus creating a potential clear-sky bias. Since low cloud type is not reported when the sky is obscured ($N = 9$), there is a similar potential sky-obscured bias. Both problems were solved by separately calculating frequencies of low cloud types, clear sky, sky-obscuring precipitation, and sky-obscuring fog where, for the purposes of this paper, sky-obscuring precipitation and sky-obscuring fog are identified as two additional ''low cloud types.''

The frequencies of occurrence of clear sky (FQ_{clr}), sky-obscuring precipitation (FQ_{sop}), and sky-obscuring fog (FQ_{fog}) were calculated by

$$FQ_{clr} = \frac{N_{clr}}{N_{all}} \qquad FQ_{sop} = \frac{N_{sop}}{N_{all}} \qquad FQ_{fog} = \frac{N_{fog}}{N_{all}}, \quad \text{(A1)}$$

where N_{clr}, N_{sop}, and N_{fog} are the total number of observations reporting clear sky, sky-obscuring precipitation, and sky-obscuring fog and N_{all} is the total number of all cloud observations, whether or not they report low cloud type. The frequencies of occurrence of low cloud types 1–9 (FQ_i where $C_L\,1 \le i \le C_L\,9$) were calculated by

$$FQ_i = \frac{N_i}{N_{low}}(1 - FQ_{clr} - FQ_{sop} - FQ_{fog}), \quad \text{(A2)}$$

where N_i is the total number of observations reporting cloud type i and N_{low} is the total number of observations that report low cloud types when the sky is not clear or obscured. The frequency of occurrence of no-low-clouded (FQ_0) was calculated by

$$FQ_0 = \frac{N_0}{N_{low}}(1 - FQ_{clr} - FQ_{sop} - FQ_{fog}) + FQ_{clr}, \quad \text{(A3)}$$

where N_0 is the total number of observations reporting $C_L\,0$. Equations (A2) and (A3) are exact and reduce to a form similar to that of (A1) in the case that low cloud types are always reported. Every possible sky condition for low cloud identification is included and $\Sigma_i\, FQ_i + FQ_0 + FQ_{sop} + FQ_{fog} = 1$.

REFERENCES

Arking, A., 1991: The radiative effects of clouds and their impact on climate. *Bull. Amer. Meteor. Soc.,* **72,** 795–813.

Bond, N. A., 1992: Observations of planetary boundary-layer structure in the eastern equatorial Pacific. *J. Climate,* **5,** 699–706.

Bretherton, C. S., 1992: A conceptual model of the stratocumulus-trade-cumulus transition in the subtropical oceans. Preprints, *Proc. 11th Int. Conf. on Clouds and Precipitation,* Vol. I, Montreal, PQ, Canada, Amer. Meteor. Soc., 374–377.

——, and R. Pincus, 1995: Cloudiness and marine boundary layer dynamics in the ASTEX Lagrangian experiments. Part I: Synoptic setting and vertical structure. *J. Atmos. Sci.,* **52,** 2707–2723.

——, and W. C. Wyant, 1997: Moisture transport, lower-tropospheric stability, and decoupling of cloud-topped boundary layers. *J. Atmos. Sci.,* **54,** 148–167.

——, P. Austin, and S. T. Siems, 1995: Cloudiness and marine boundary layer dynamics in the ASTEX Lagrangian experiments. Part II: Cloudiness, drizzle, surface fluxes, and entrainment. *J. Atmos. Sci.,* **52,** 2724–2735.

Curry, J. A., E. E. Ebert, and G. F. Herman, 1988: Mean and turbulence structure of the summertime Arctic cloudy boundary layer. *Quart. J. Roy. Meteor. Soc.,* **114,** 715–746.

Deser, C., and J. M. Wallace, 1990: Large-scale atmospheric circulation features of warm and cold episodes in the tropical Pacific. *J. Climate,* **3,** 1254–1281.

——, J. J. Bates, and S. Wahl, 1993: The influence of sea surface temperature gradients on stratiform cloudiness along the equatorial front in the Pacific Ocean. *J. Climate,* **6,** 1172–1180.

Goerss, J. S., and C. E. Duchon, 1980: Effect of ship heating on dry-bulb temperature measurements in GATE. *J. Phys. Oceanogr.,* **10,** 478–479.

Hahn, C. J., S. G. Warren, J. London, R. L. Jenne, and R. M. Chervin, 1988: Climatological data for clouds over the globe from surface observations. Carbon Dioxide Information Analysis Center Rep. NDP-026, Oak Ridge National Laboratory, Oak Ridge, TN, 54 pp. [Available from Carbon Dioxide Analysis Center, Oak Ridge National Laboratory, P.O. Box 2008, Oak Ridge, TN 37831-6335.]

——, ——, and ——, 1995: The effect of moonlight on observation of cloud cover at night, and application to cloud climatology. *J. Climate,* **8,** 1429–1446.

——, ——, and ——, 1996: Edited synoptic cloud reports from ships and land stations over the globe, 1982–1991. Carbon Dioxide Information Analysis Center Rep. NDP026B, 45 pp. [Available from Carbon Dioxide Information Analysis Center, Oak Ridge National Laboratory, P.O. Box 2008, Oak Ridge, TN 37831-6335.]

Hanson, H. P., 1991: Marine stratocumulus climatologies. *Int. J. Climatol.,* **11,** 147–164.

Haraguchi, P. Y., 1968: Inversions over the tropical eastern Pacific Ocean. *Mon. Wea. Rev.,* **96,** 177–185.

Hartmann, D. L., M. E. Ockert-Bell, and M. L. Michelsen, 1992: The effect of cloud type on Earth's energy balance: Global analysis. *J. Climate,* **5,** 1281–1304.

Herman, G., and R. Goody, 1976: Formation and persistence of summertime Arctic stratus clouds. *J. Atmos. Sci.,* **33,** 1537–1553.

Hoskins, B. J., H. H. Hsu, I. N. James, M. Masutani, P. D. Sardeshmukh, and G. H. White, 1989: Diagnostics of the global atmospheric circulation based on ECMWF analyses 1979–1989. WCRP-27, WMO/TD No. 326., WMO, 219 pp.

Houze, R. A., 1993: *Cloud Dynamics.* Academic Press, 573 pp.

Klein, S. A., and D. L. Hartmann, 1993: The seasonal cycle of low stratiform clouds. *J. Climate,* **6,** 1587–1606.

——, ——, and J. R. Norris, 1995: On the relationship among low-

cloud structure, sea surface temperature, and atmospheric circulation in the summertime northeast Pacific. *J. Climate,* **8,** 1140–1155.

Lilly, D. K., 1968: Models of cloud-topped mixed layers under a strong inversion. *Quart. J. Roy. Meteor. Soc.,* **94,** 292–309.

Mitchell, T. P., and J. M. Wallace, 1992: The annual cycle in equatorial convection and sea surface temperature. *J. Climate,* **5,** 1140–1156.

Neiburger, M., D. S. Johnson, and C.-W. Chien, 1961: *Studies of the Structure of the Atmosphere over the Eastern Pacific Ocean in Summer*. Vol. 1, *The Inversion over the Eastern North Pacific Ocean.* University of California Press, 94 pp.

Norris, J. R., 1998: Low cloud type over the ocean from surface observations. Part I: Relationship to surface meteorology and the vertical distribution of temperature and moisture. *J. Climate,* **11,** 369–382.

——, and C. B. Leovy, 1994: Interannual variability in stratiform cloudiness and sea surface temperature. *J. Climate,* **7,** 1915–1925.

Orville, R. E., and R. W. Henderson, 1986: Global distribution of midnight lightning: September 1977 to August 1987. *Mon. Wea. Rev.,* **114,** 2640–2653.

Petty, G. W., 1995: Frequencies and characteristics of global oceanic precipitation from shipboard present-weather reports. *Bull. Amer. Meteor. Soc.,* **76,** 1593–1616.

Rossow, W. B., and R. A. Schiffer, 1991: ISCCP cloud data products. *Bull. Amer. Meteor. Soc.,* **72,** 2–20.

Rozendaal, M. A., C. B. Leovy, and S. A. Klein, 1995: An observational study of diurnal variations of marine stratiform cloud. *J. Climate,* **8,** 1795–1809.

Schubert, W. H., J. S. Wakefield, E. J. Steiner, and S. K. Cox, 1979: Marine stratocumulus convection. Part II: Horizontally inhomogeneous solutions. *J. Atmos. Sci.,* **36,** 1308–1324.

Wallace, J. M., T. P. Mitchell, and C. Deser, 1989: The influence of sea-surface temperature on surface wind in the eastern equatorial Pacific: Seasonal and interannual variability. *J. Climate,* **2,** 1492–1499.

Warren S. G., C. J. Hahn, J. London, R. M. Chervin, and R. L. Jenne, 1988: Global distribution of total cloud cover and cloud type amounts over the ocean. NCAR/TN-317+STR, Boulder, CO, 42 pp. plus 170 maps. [Available from NCAR, P.O. Box 3000, Boulder, CO 80307.]

Woodruff, S. D., R. J. Slutz, R. L. Jenne, and P. M. Steurer, 1987: A Comprehensive Ocean–Atmosphere Data Set. *Bull. Amer. Meteor. Soc.,* **68,** 1239–1250.

WMO, 1974: Manual on codes. WMO Publ. 306, WMO.

——, 1975: Manual on the observation of clouds and other meteors. WMO Publ. 407, WMO, 155 pp.

Wyant, M. C., C. S. Bretherton, H. A. Rand, and D. E. Stevens, 1997: Numerical simulations and a conceptual model of the stratocumulus to trade cumulus transition. *J. Atmos. Sci.,* **54,** 168–192.